

LIBRARY  
ROYAL AIRCRAFT ESTABLISHMENT  
BEDFORD.



MINISTRY OF AVIATION  
AERONAUTICAL RESEARCH COUNCIL  
*CURRENT PAPERS*

# Approximate Formulae for the Lift and Drag of Wedge Aerofoil Sections at High Supersonic Speeds

By  
L. C. Squire

LONDON: HER MAJESTY'S STATIONERY OFFICE

1966

Price 3s. 6d. net



Approximate Formulae for the Lift and  
Drag of Wedge Aerofoil Sections at  
High Supersonic Speeds

---

by

L. C. Squire

Engineering Laboratory, University of Cambridge

Summary

In this paper a correlation derived by Bertram & Cook is used to obtain approximate formulae for the aerodynamic derivatives of simple wedge aerofoils for a wide range of Mach number and incidence. The correlation allows equilibrium real gas effects to be included in an approximate manner.



## 1. Introduction

At high supersonic speed the initial normal-force curve slope of a simple wedge section may be many times greater than that of the equivalent flat plate. This fact obviously has great significance in the design of isolated controls. In connection with this interest Edwards<sup>1</sup> has pointed out that existing tables and charts for the properties of oblique shock waves are inconvenient for the rapid evaluation of the aerodynamic derivatives of these sections. To overcome this difficulty he has tabulated the surface pressures on a series of wedges for the Mach number range  $M = 2.0$  to  $M = 15$ . These pressures were obtained from the exact oblique shock relations assuming inviscid flow and neglecting real gas effects. From these pressures Edwards has calculated (by numerical differentiation) normal-force curve slopes and lift curve slopes of wedges for a series of leading-edge angles over a wide Mach number range. The incidence is, however, limited to angles less than the wedge semi-angle since the theory only includes compression surfaces.

At the same time as Edwards' paper was published Bertram & Cook<sup>2</sup> published a report concerned with the correlation of the flow properties across oblique shock waves and expansion waves for a range of specific-heat ratios. In the present paper these correlations are used to derive approximate formulae for the aerodynamic derivatives of wedge aerofoils. As the correlation includes equilibrium real gas effects the formulae presented here cover a very wide range of flight conditions. However, the results still ignore viscous effects and these become increasingly important at the higher Mach number. The approximate results are found to be in close agreement with the numerical results of Edwards.

In addition to their interest in connection with the design of isolated controls the results for wedge aerofoils may be of value in two other fields of current interest. One of these arises from the fact that in the upper part of the speed range for air-breathing engines the exit area of the jet nozzle tends to be much greater than the intake stream-tube. This means that integration of these engines with the aircraft usable volume results in overall cross-sectional area distributions with bluff bases<sup>3</sup>. (These bluff bases are, of course, filled by the jet in the cruise condition). A study of the properties of wedge aerofoil sections may provide some data on the influence of finite bases on the non-linear aerodynamic characteristics of this type of integrated aircraft. The second field concerns the design of three-dimensional lifting shapes from the two-dimensional flow field through an oblique shock wave<sup>4</sup>. For such shapes the aerodynamic derivatives close to design presumably will be the same as on the corresponding wedge.

Notation

$C_A$	axial force coefficient
$C_D$	drag coefficient
$C_L$	lift coefficient
$C_N$	normal force coefficient
$\bar{K}$	$M\theta$
$K$	$M^2 \sin\theta/\beta$
$M$	Mach number
$M_N$	Mach number normal to shock
$p$	static pressure
$P, P_e$	non-dimensional pressures (see eqns. (2) and (7))
$X, X_e$	correlating functions (see eqns. (2) and (7))
$\alpha$	incidence
$\beta$	$(M^2 - 1)^{\frac{1}{2}}$
$\gamma$	ratio of specific heats
$\gamma_e$	effective isentropic exponent (see eqn. (5))
$\delta$	wedge semi-angle
$\theta$	flow deflection angle
$\eta$	shock angle
$\rho$	density

Suffices

L	lower surface
U	upper surface
$\infty$	free stream conditions

## 2. The Correlation of Bertram & Cook

### Compression Surface

The normal hypersonic approximation for the pressure  $p$  at a point on the surface of a plate inclined to a stream at an angle  $\theta$  may be written -

$$\left(\frac{p}{p_\infty} - 1\right) = \frac{\gamma(\gamma + 1)}{4} \bar{K}^2 + \gamma \bar{K} \left[1 + \left(\frac{\gamma + 1}{4} \bar{K}\right)^2\right]^{\frac{1}{2}} \quad (1)$$

where  $\bar{K} = M\theta$ , and  $p$ ,  $\gamma$  and  $M$  are the static pressure, the ratio of specific heats, and Mach number, respectively, in the free stream. Following Ivey & Cline<sup>5</sup>, Bertram & Cook replace  $\bar{K} = M\theta$  in Eqn. (1) by  $M^2 \sin\theta/\beta$ ,  $\left[=(M^2 \sin\theta/(M^2 - 1)^{\frac{1}{2}})\right]$  so that Eqn. (1) joins up with linear theory, and also has the right form if it is assumed that  $\sin\theta \doteq \tan\theta$ . With this modification to the hypersonic similarity parameter Eqn. (1) may be written

$$P = X^2 + X\sqrt{1 + X^2}, \quad (2)$$

where  $P = \frac{\gamma + 1}{4\gamma} \left(\frac{p}{p_\infty} - 1\right)$ ,  $X = \frac{\gamma + 1}{4} \frac{M^2}{\beta} \sin\theta$ .

To the same approximation the relationship between shock angle ( $\eta$ ) and deflection angle ( $\theta$ ) is

$$M \sin \eta = M_N = X + \sqrt{1 + X^2}. \quad (3)$$

Bertram & Cook plot the equivalent of  $P$  against  $X^*$  for a large number of exact solutions covering the range  $1.1 \leq M \leq 40$  and  $1 \leq \gamma \leq 5/3$ . These exact solutions are in excellent agreement with Eqn. (2) for a wide range of  $X$ . At given Mach number the exact solutions diverge from Eqn. (2) above a certain value of  $X$ , this value of  $X$  being higher at lower values of  $\gamma$ . The incidences above which the approximate formula differs from the exact results by more than 5% are plotted in Fig. 1. This figure also includes the shock detachment angle. As can be seen the approximate formula is adequate to within a few degrees of the shock detachment for all Mach numbers and values of  $\gamma$ .

---

\* Actually  $K_p$  ( $= 4P$ ) against  $K_\gamma$  ( $= 4X$ ).

### Expansion Surfaces

For sudden expansions (i.e. centred Prandtl-Meyer waves) Bertram & Cook have again plotted exact results in the form of P against X. Again there is good correlation, particularly at higher Mach numbers, but now the best agreement is obtained at the higher specific heat ratios. Above Mach numbers of 2.0 the results lie close to the line given by

$$\frac{p}{p_{\infty}} = \left(1 + \frac{\gamma - 1}{2} K\right)^{\frac{2\gamma}{\gamma - 1}}, \quad (4)$$

or in the present notation

$$P = \frac{\gamma + 1}{4} \left(1 + \frac{2(\gamma - 1)}{\gamma + 1} X\right)^{\frac{2\gamma}{\gamma - 1}} - \frac{\gamma + 1}{4}.$$

In general the collapse of the expansion results is less satisfactory than that of the compression results. However, in calculating aerodynamic characteristics this is not important since the contributions of suction surfaces become very small at high supersonic speeds.

### Real Gas Effects

To include real gas effects Bertram & Cook follow Trimpi & Jones<sup>6</sup> in defining an effective value of the isentropic exponent  $\gamma_e$  to describe the density changes across an oblique shock wave so that the above correlation can be applied to a real gas in equilibrium.  $\gamma_e$  is defined by

$$\gamma_e = 2 \left[ \frac{1/M_N^2 - 1}{\frac{\rho_{\infty}}{\rho} - 1} \right] - 1, \quad (5)$$

where  $M_N$  is Mach number normal to the shock and  $\rho$  the density behind the shock. Values of  $\gamma_e$  as a function of  $M_N$  for various altitudes in the atmosphere are plotted in Fig. 12 of Ref. 2.

Then, using a similar analysis to that used to derive Eqns. (2) and (3), it is found that

$$M_N = X_e + \sqrt{1 + X_e^2}, \quad (6)$$

and

$$\frac{\gamma_e}{\gamma} P_e = X_e^2 + X_e \sqrt{1 + X_e^2}, \quad (7)$$



where  $P_e = \frac{\gamma_e + 1}{4 \gamma_e} \left( \frac{p}{p_\infty} - 1 \right)$  and  $X_e = \frac{\gamma_e + 1}{4} \frac{M^2}{\beta} \sin \theta$ .

### 3. Aerodynamic Derivatives

For the wedge aerofoil of unit chord shown in Fig. 2 the normal-force coefficient is given by

$$C_N = \frac{1}{q} (p_L - p_U) = \frac{2}{\gamma M^2} \left( \frac{p_L}{p_\infty} - \frac{p_U}{p_\infty} \right), \quad (8)$$

and the axial-force coefficient by

$$C_A = \frac{2}{\gamma M^2} \left( \frac{p_L}{p_\infty} + \frac{p_U}{p_\infty} - \frac{2p_B}{p_\infty} \right) \tan \delta. \quad (9)$$

Here  $p_L$  and  $p_U$  are the pressures on the lower and upper surfaces respectively,  $p_B$  is the base pressure and  $\delta$  the wedge semi-angle. At incidence  $\alpha$ , the lift and drag coefficients are related to  $C_N$  and  $C_A$  in the usual manner, and the normal-force-curve slope and lift-curve slope are given by

$$\frac{\partial C_N}{\partial \alpha} = \frac{2}{\gamma M^2} \left[ \frac{\partial}{\partial \alpha} \left( \frac{p_L}{p_\infty} \right) - \frac{\partial}{\partial \alpha} \left( \frac{p_U}{p_\infty} \right) \right], \quad (10)$$

$$\text{and } \frac{\partial C_L}{\partial \alpha} = \frac{2}{\gamma M^2 \cos \delta} \left[ \cos(\alpha + \delta) \frac{\partial}{\partial \alpha} \left( \frac{p_L}{p_\infty} \right) - \cos(\delta - \alpha) \frac{\partial}{\partial \alpha} \left( \frac{p_U}{p_\infty} \right) \right] - C_D, \quad (11)$$

where  $p_B$  is assumed independent of  $\alpha$ .

Values of  $\frac{p}{p_\infty}$  and  $\frac{\partial}{\partial \alpha} \left( \frac{p}{p_\infty} \right)$  can be found from Eqns. (2), (4) or (7) depending on the relative values of  $\alpha$  and  $\delta$ , and on the physical conditions. The results for the different cases are as follows.

#### 3.1 Perfect gases

If  $\alpha < \delta$ , both surfaces of the wing are compression surfaces and Eqn. (2) gives

$$\frac{p}{p_{\infty}} = 1 + \frac{4\gamma}{1+\gamma} \left[ X^2 + X(1+X^2)^{\frac{1}{2}} \right], \quad (12)$$

$$\frac{\partial}{\partial \alpha} \left( \frac{p}{p_{\infty}} \right) = \mp \frac{\gamma M^2}{\beta} \left[ 2X + (1+2X^2)/(1+X^2)^{\frac{1}{2}} \right] \cos(\delta \mp \alpha) \quad (13)$$

where  $X = \frac{\gamma+1}{4} \frac{M^2}{\beta} \sin(\delta \mp \alpha)$ , and the negative sign refers to the upper surface ( $\delta - \alpha$ ), and the positive sign to the lower surface ( $\delta + \alpha$ ).

When  $\alpha > \delta$  we can still use Eqns. (12) and (13) for the lower surface, but must now use Eqn. (4) for the upper, suction, surface to get

$$\frac{p_U}{p_{\infty}} = \left( 1 + \frac{2(\gamma-1)}{\gamma+1} X \right)^{\frac{2\gamma}{\gamma-1}}, \quad (14)$$

$$\frac{\partial}{\partial \alpha} \left( \frac{p_U}{p_{\infty}} \right) = \frac{\gamma M^2}{\beta} \cos(\delta - \alpha) \left( 1 + \frac{2(\gamma-1)}{\gamma+1} X \right)^{\frac{\gamma+1}{\gamma-1}}, \quad (15)$$

where  $X = \frac{\gamma+1}{4} \frac{M^2}{\beta} \sin(\delta - \alpha)$ .

For the flat plate at incidence  $\alpha$  the formula for  $\frac{\partial C_N}{\partial \alpha}$  reduces to the simple form

$$\frac{\partial C_N}{\partial \alpha} = \frac{2}{\beta} \left[ 2X + (1+2X^2)/(1+X^2)^{\frac{1}{2}} + \left( 1 + \frac{2(\gamma-1)}{\gamma+1} X \right)^{\frac{\gamma+1}{\gamma-1}} \right] \cos \alpha \quad (16)$$

( $X = \frac{\gamma+1}{4} \frac{M^2}{\beta} \sin \alpha$ ),

and for the wedge of semi-angle  $\delta$  at zero incidence to

$$\frac{\partial C_N}{\partial \alpha} = \frac{4}{\beta} \left[ 2X + (1+2X^2)/(1+X^2)^{\frac{1}{2}} \right] \cos \delta \quad (17)$$

( $X = \frac{\gamma+1}{4} \frac{M^2}{\beta} \sin \delta$ ).

For fixed Mach number  $X \rightarrow 0$  as  $\alpha \rightarrow 0$ , or  $\delta \rightarrow 0$  so that in both cases  $\frac{\partial C_N}{\partial \alpha}$  tends to  $4/\beta$ , the linear theory value.

### 3.2 Real gas effects

Where real gas effects are present Eqn. (7) can be used for the surface pressure, provided the effective value of  $\gamma_e$  can be found. For flight in the atmosphere  $\gamma_e$  is given as a function of  $M_N$  and height in Fig. 12 of Ref. 2. Thus, for a given wedge angle at given Mach number and height,  $\gamma_e$  can be found from this figure in conjunction with the relationship between  $M_N$  and  $X_e$  (Eqn. (6)) and the definition of  $X_e$  (Eqn. (7)).

The derivative  $\frac{\partial}{\partial \alpha} \left( \frac{p}{p_\infty} \right)$ , required to find  $\frac{\partial C_N}{\partial \alpha}$  and  $\frac{\partial C_L}{\partial \alpha}$ , can be found by direct differentiation of Eqn. (7), provided it is assumed that the relaxation time of the gas is small, i.e. that a change in incidence results in an instantaneous change in equilibrium state. Thus for  $\alpha < \delta$ ,

$$\begin{aligned} \frac{\partial}{\partial \alpha} \left( \frac{p}{p_\infty} \right) = \mp \frac{\gamma M^2}{\beta} \cos(\delta \mp \alpha) \left\{ 2X_e + \frac{1 + 2X_e^2}{\sqrt{1 + X_e^2}} \right\} \\ + \frac{4\gamma}{(\gamma_e + 1)^2} \left( X_e^2 + \frac{X_e^3}{\sqrt{1 + X_e^2}} \right) \frac{\partial \gamma_e}{\partial \alpha}, \end{aligned} \quad (18)$$

where, again, the negative sign refers to the upper surface and the positive sign to the lower surface. Using the fact that  $\gamma_e$  is a function only of  $M_N$  at fixed height (and so by Eqn. (6) a function of  $X_e$  only) we obtain

$$\frac{\partial \gamma_e}{\partial \alpha} = \frac{\partial \gamma_e}{\partial X_e} \left[ \frac{X_e}{1 + \gamma_e} \frac{\partial \gamma_e}{\partial \alpha} \mp X_e \cot(\delta \mp \alpha) \right], \quad (19)$$

or

$$\frac{\partial \gamma_e}{\partial \alpha} = \mp \frac{\frac{\partial \gamma_e}{\partial X_e} X_e \cot(\delta \mp \alpha)}{1 - \frac{\partial \gamma_e}{\partial X_e} \cdot \frac{X_e}{1 + \gamma_e}}. \quad (20)$$

After substitution for  $\partial\gamma_e/\partial\alpha$  from (20), Eqn. (18) reduces to

$$\frac{\partial}{\partial\alpha} \left( \frac{p}{p_\infty} \right) = \bar{\gamma} \frac{\gamma M^2}{\beta} \cos(\delta + \alpha) \left( 2X_e + \frac{1 + 2X_e^2}{\sqrt{1 + X_e^2}} \right) (1 + \epsilon), \quad (21)$$

where

$$\epsilon = \frac{\frac{\partial\gamma_e}{\partial X_e} X_e^2 \left( 1 + \frac{X_e}{\sqrt{1 + X_e^2}} \right)}{\left( 1 + \gamma_e - X_e \frac{\partial\gamma_e}{\partial X_e} \right) \left( 2X_e + \frac{1 + 2X_e^2}{\sqrt{1 + X_e^2}} \right)}. \quad (22)$$

The function  $\epsilon$ , which defines the effects of changes in the equilibrium conditions, is plotted in Fig. 3. As can be seen the effects are small. For finite relaxation times we may expect the effective value of  $\epsilon$  to be initially smaller than that given by (22), and to approach this value after the incidence change. However, since  $\epsilon$  is small this is not likely to be an important effect.

In the case where  $\alpha > \delta$  we may use Eqn. (4) directly to find  $\left( \frac{p}{p_\infty} \right)$  for the upper surface since real gas effects are likely to be less important, also, as pointed out earlier, the suction force on this surface makes only a small contribution to the overall force.

#### 4. Discussion of Results

##### 4.1 Comparison with Edwards' numerical solution

In his paper Edwards has tabulated the ratio

$$\left( \left( \frac{\partial C_N}{\partial\alpha} \right)_{\delta=0} \right)_{\alpha=0} \bigg/ \left( \frac{\partial C_N}{\partial\alpha} \right)_{\delta=0} \quad \text{for wedge angles up to } 20^\circ \text{ and Mach}$$

numbers between 2.0 and 15.0. In the approximate theory of this paper this ratio is given by

$$\left( 2X + \frac{(1 + 2X^2)}{(1 + X^2)^{\frac{1}{2}}} \right) \cos \delta, \quad \text{where } X = \frac{\gamma + 1}{4} \frac{M^2}{\beta} \sin \delta. \quad (23)$$

Sample comparisons covering the range computed by Edwards are shown in the following Table.

M	$\delta = 6^\circ$		$\delta = 12^\circ$		$\delta = 20^\circ$	
	Ref. 1	Eqn. 23	Ref. 1	Eqn. 23	Ref. 1	Eqn. 23
2	1.30	1.31	1.69	1.66	2.83	2.12
5	1.76	1.77	2.70	2.73	4.03	4.04
10	2.75	2.76	4.97	4.98	7.84	7.87
15	3.88	3.89	7.38	7.37	11.72	11.70

As can be seen the agreement is excellent, as of course might be expected from the success of the basic correlation as indicated in Fig. 1.

#### 4.2 Comparison of various types of aerofoil section

The results tabulated above show that the initial normal-force curve slope of a simple wedge aerofoil increases rapidly with increase in wedge angle, particularly at higher Mach numbers. This increase in normal force is accompanied by an increased axial, or chordwise force. However, it should be noted that the normal-force-curve slope increases less rapidly with incidence at larger wedge angles than it does for the flat plate. Thus at given incidence the ratio of normal force, or lift, on wedges of different leading edge angles may be much smaller than indicated by the ratio of initial normal-force-curve slopes. These effects are illustrated in Figs. 4 and 5, where lifts of wedges of semi-angles of  $0^\circ$ ,  $5^\circ$  and  $10^\circ$  are compared at Mach numbers of 5 and 10. The lift-curve of the  $10^\circ$  wedge is almost straight, in fact at  $M = 5$  there is a slight fall in slope with increasing incidence. On the other hand the lift-curve of the flat plate is highly non-linear so that at  $\alpha = 20^\circ$  its lift-curve slope is the same as that of the  $10^\circ$  wedge, although its actual lift is only about half that of the wedge. The corresponding drag results are also presented in Figs. 4 and 5. (In calculating the drag the skin friction has been ignored and the base pressure has been taken as 0.5 of free stream static pressure). At low lift the drag increases with wedge angle, but at higher lifts the larger value of  $C_L/\alpha$  for the thicker wedges results in a lower lift-dependent drag so that above a particular  $C_L$ , which depends on Mach number, the drag is virtually independent of wedge angle. Looked at from another point of view, above a particular  $C_L$  the main contributor to the lift and drag comes from the lower surface; the pressure on this surface depends only on the local incidence, but is independent of the actual wedge angle.

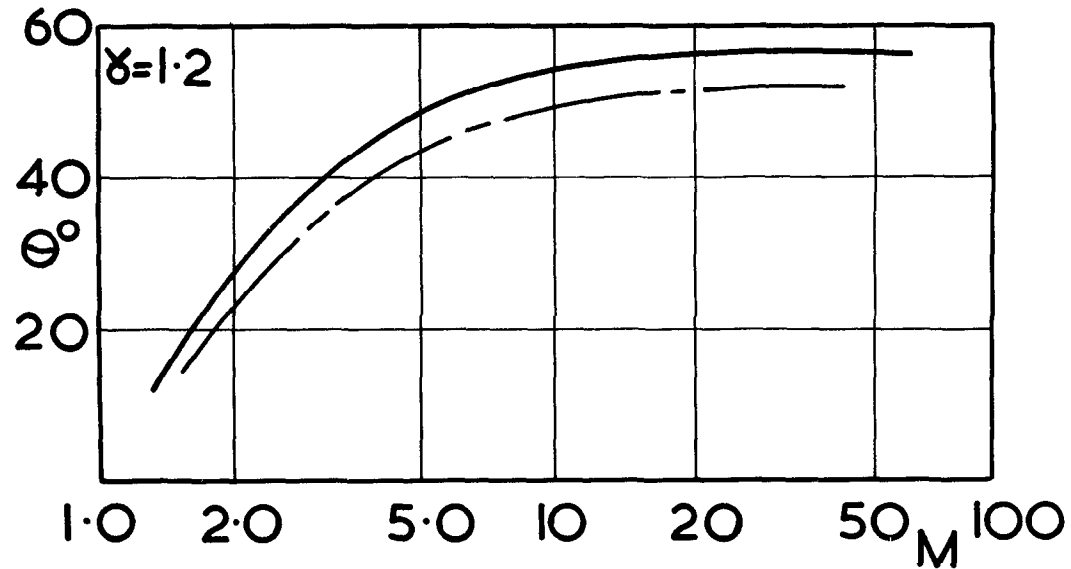
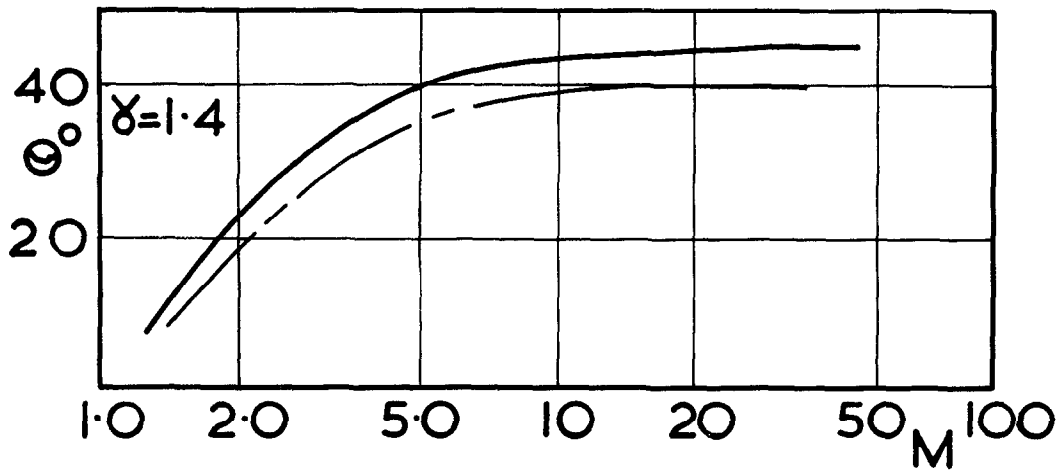
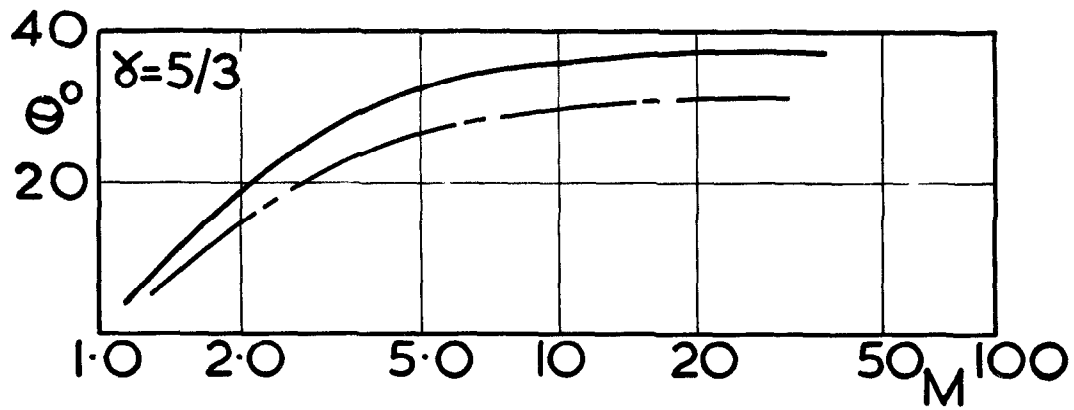
Fig. 4 also includes some results\* for a symmetrical double wedge aerofoil with a leading-edge semi-angle of  $10^\circ$ ; that is it has approximately the same cross-sectional area as the simple wedge of  $5^\circ$  semi-angle. As can be seen the double wedge has a lower lift-curve slope and a higher drag than the corresponding wedge. The lower lift arises from the fact that whereas the front of the double wedge produces much more lift than the front of the single wedge, the rear of the double wedge produces very little lift. The lower drag of the single wedge is due to its effective smaller thickness-chord ratio.

### References

1. Edwards, J.B.W. 1963 Some properties of wedge section aerofoils at supersonic and hypersonic speeds. Aero. Res. Council. 25,738. (Unpublished).
2. Bertram, M.H. & Cook, B.S. 1963 The correlation of oblique shock parameters for ratios of specific heats from 1 to  $5/3$  with applications to real gas flows. NASA Rep. no. R-171.
3. Squire, L.C. 1963 The use of excess engine exit area over intake area to reduce zero-lift drag at high supersonic speeds. Aero. Res. Council. 25,838; to be published in Aero. Quart.
4. Nonweiler, T.R.F. 1963 Delta wings of shapes amenable to exact shock-wave theory. J. Roy. Aero. Soc. Vol. LXVII, p.39.
5. Ivey, H.R. & Cline, C.W. 1950 Effects of heat-capacity lag on the flow through oblique shock waves. NACA TN 2196.
6. Trimpi, R.L. & Jones, R.A. 1960 A method of solution with tabulated results for the attached oblique shock-wave system for surfaces at various angles of attack, sweep, and dihedral in an equilibrium real gas including the atmosphere. NASA Rep. no. R-63.

---

\* These results were obtained using exact theory as the correlation of section 2 does not apply to the rear surfaces of the double wedge.



——— Shock Detachment  
 - - - 5% Error in Correlation

**FIG. 1 UPPER LIMIT OF CORRELATION**

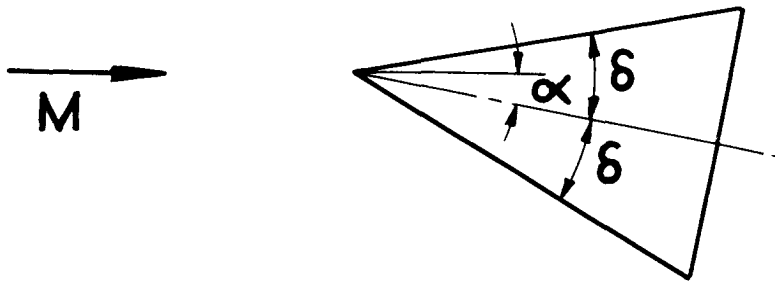


FIG. 2 NOTATION

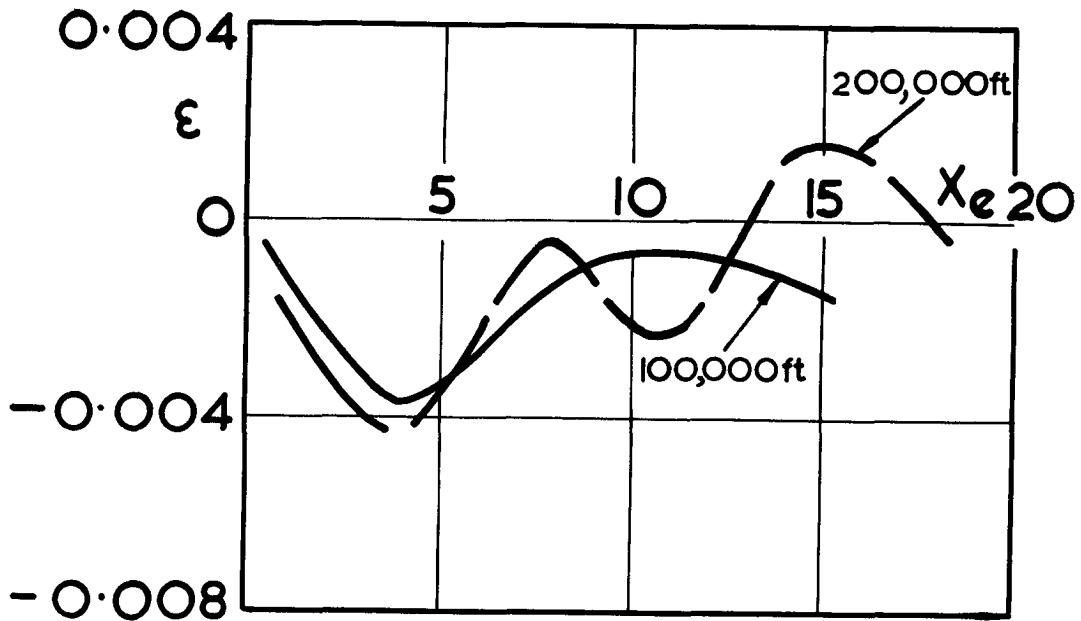


FIG. 3 VARIATION OF  $\epsilon$  WITH  $X_e$



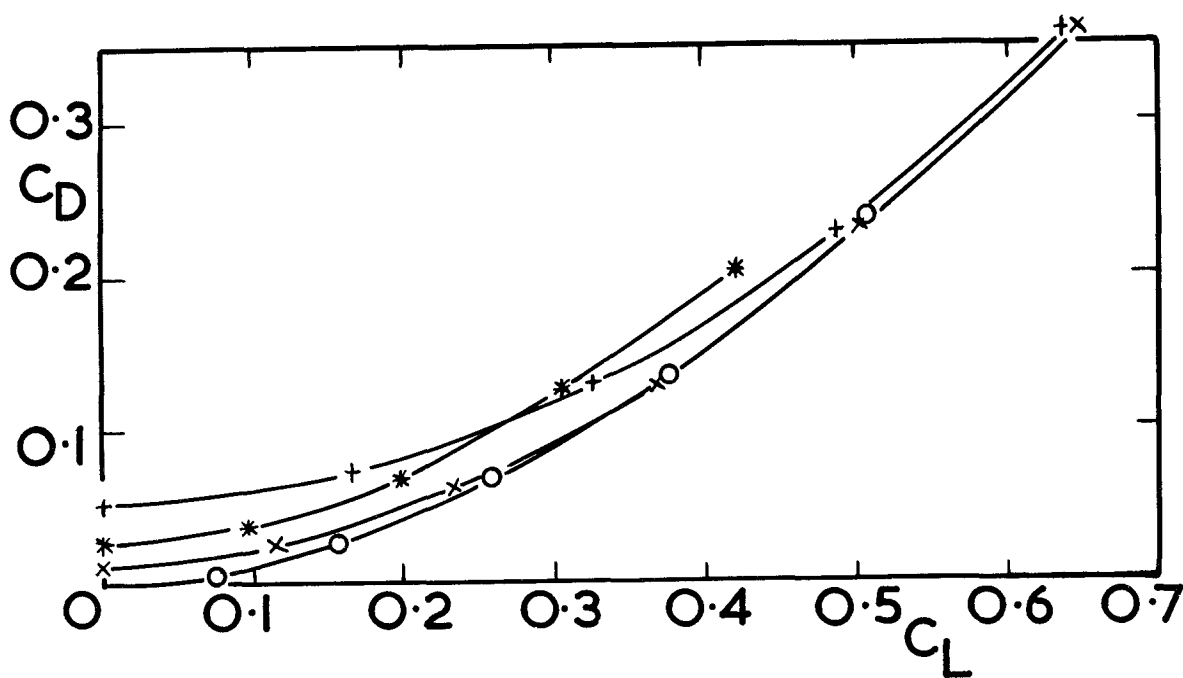
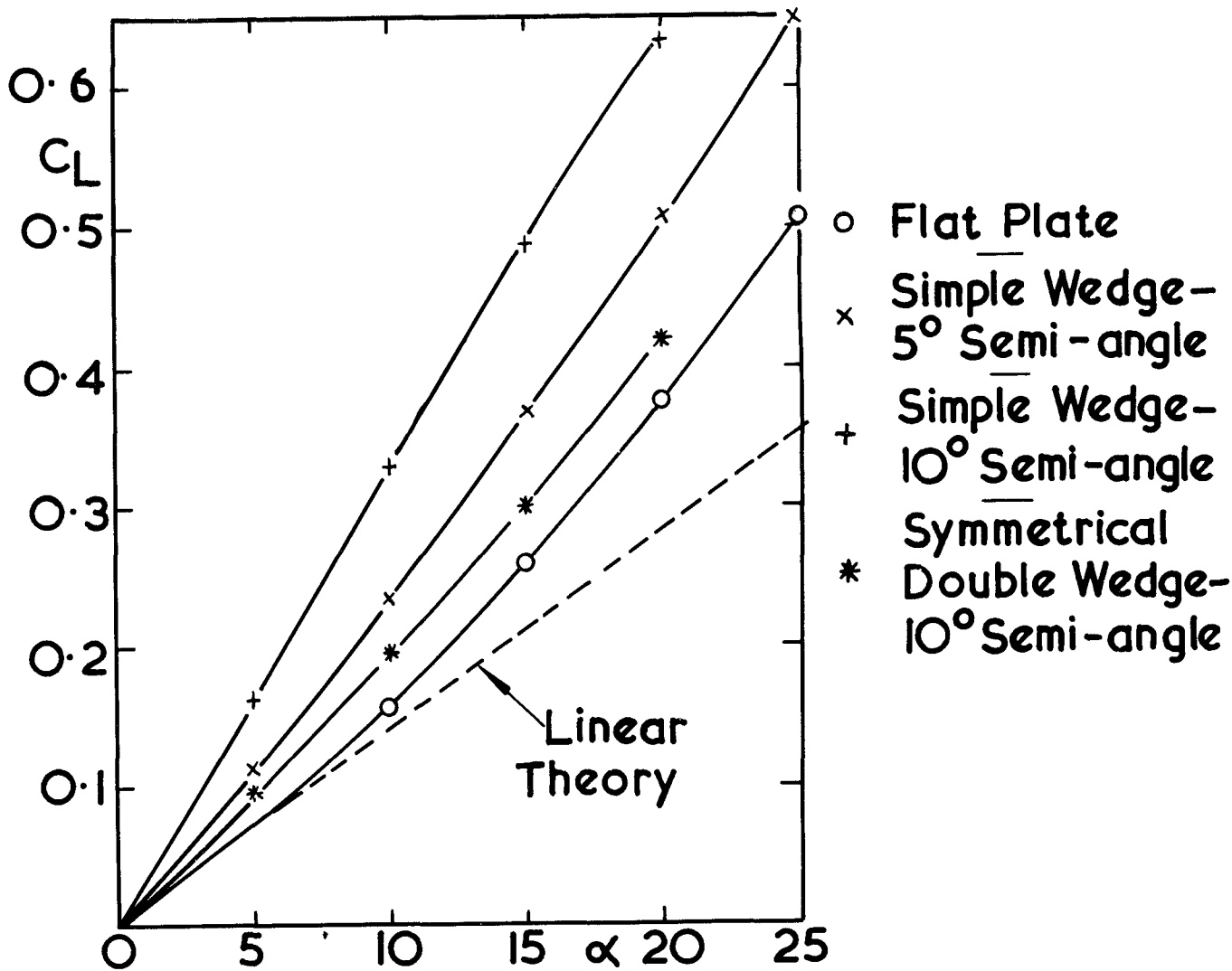
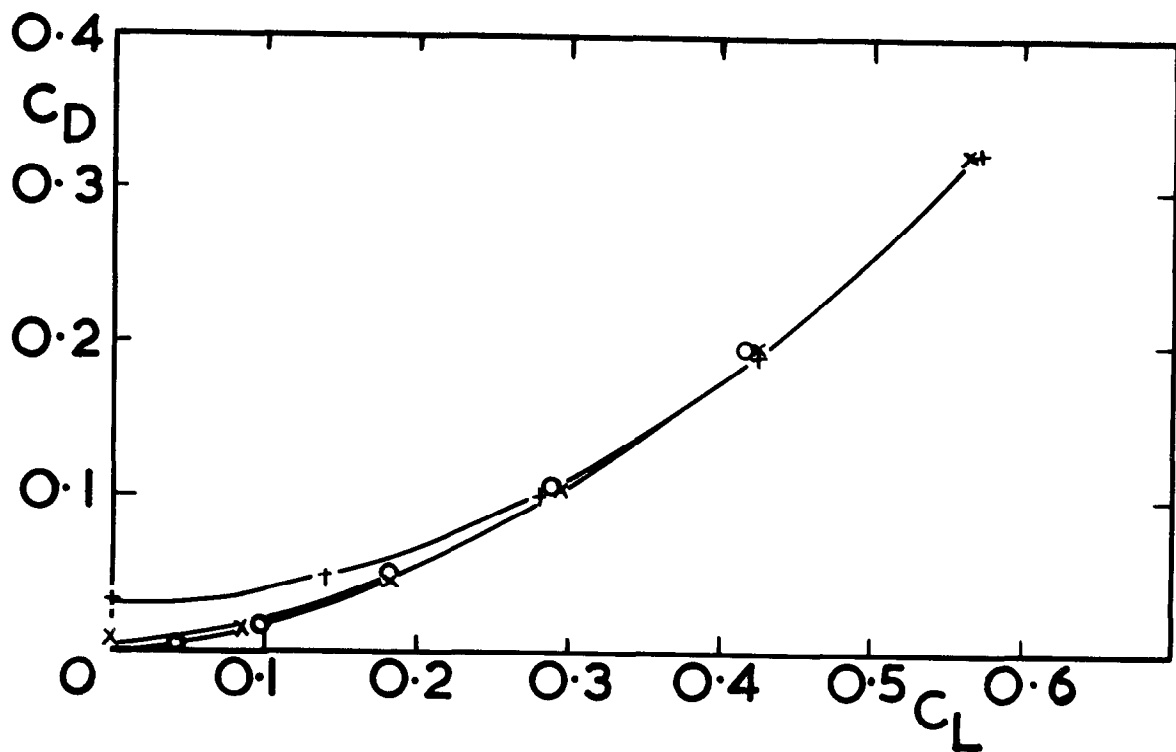
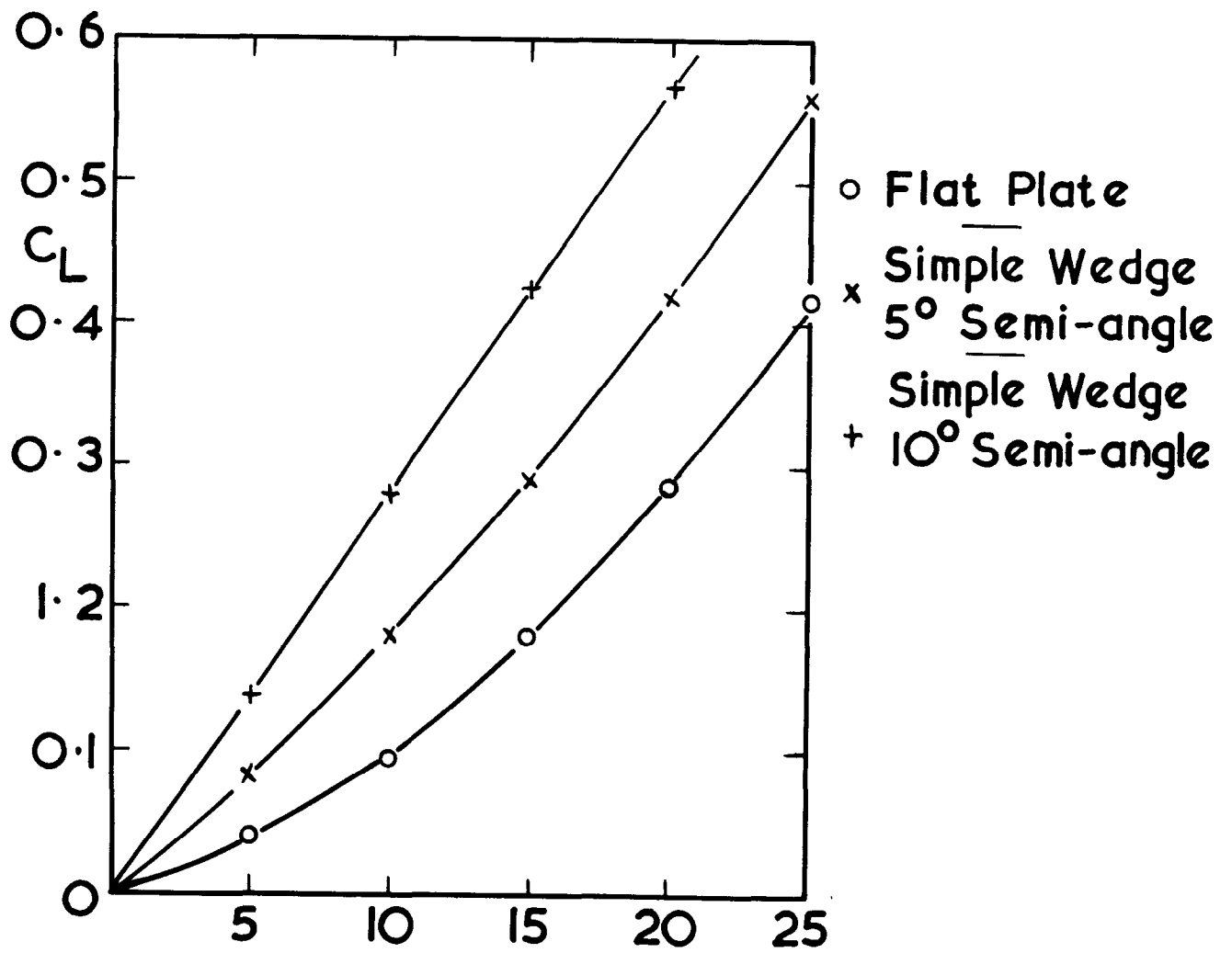


FIG. 4 COMPARISON OF VARIOUS SIMPLE AEROFOIL SECTIONS AT  $M = 5.0$



**FIG. 5** COMPARISON OF VARIOUS SIMPLE AEROFOIL SECTIONS AT  $M = 10$

A.R.C. C.P. No. 864  
March 1965  
Squire, L. C.

APPROXIMATE FORMULAE FOR THE LIFT AND  
DRAG OF WEDGE AEROFOIL SECTIONS AT  
HIGH SUPERSONIC SPEEDS

In this paper a correlation derived by Bertram & Cook is used to obtain approximate formulae for the aerodynamic derivatives of simple wedge aerofoils for a wide range of Mach number and incidence. The correlation allows equilibrium real gas effects to be included in an approximate manner.

A.R.C. C.P. No. 864  
March 1965  
Squire, L. C.

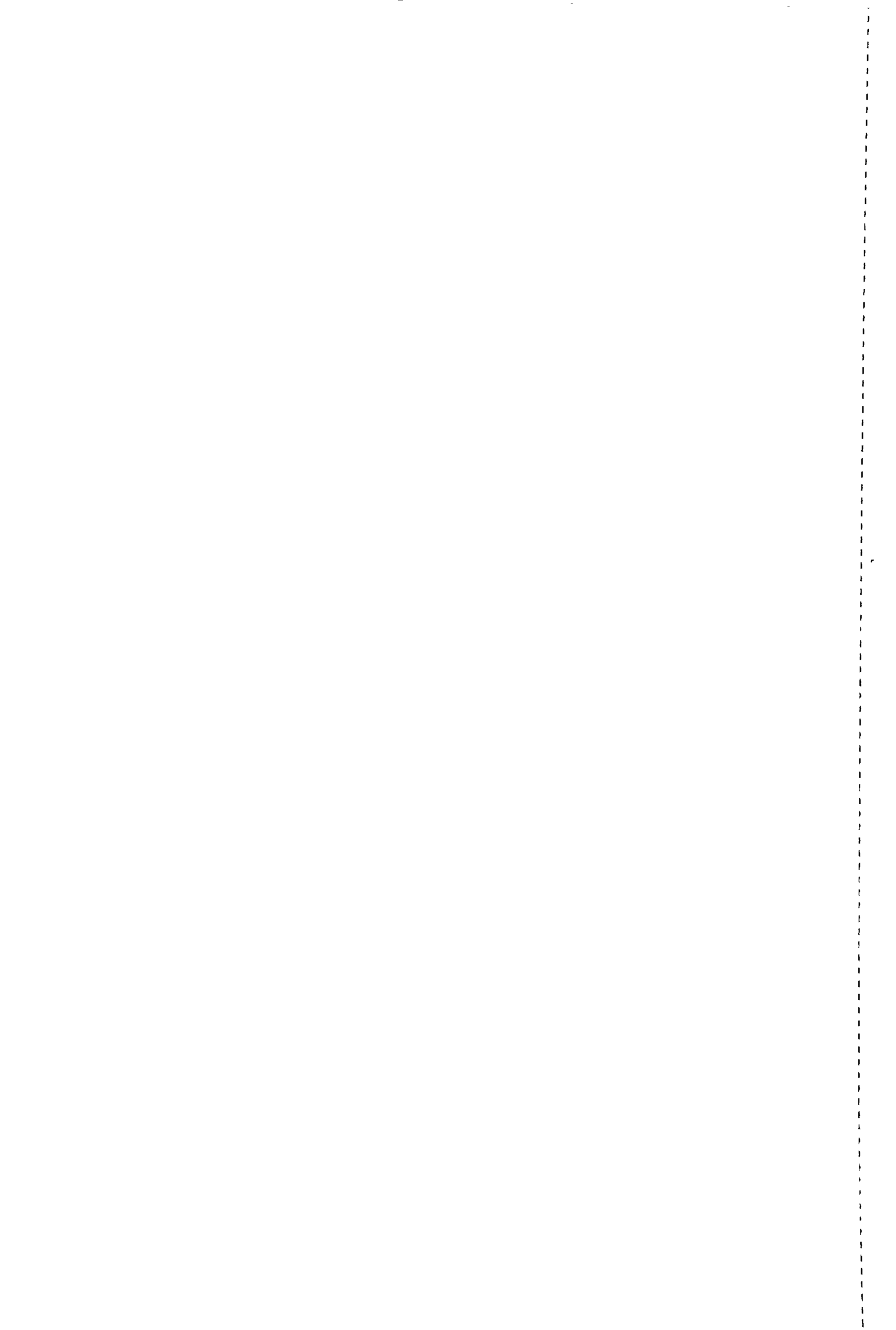
APPROXIMATE FORMULAE FOR THE LIFT AND  
DRAG OF WEDGE AEROFOIL SECTIONS AT  
HIGH SUPERSONIC SPEEDS

In this paper a correlation derived by Bertram & Cook is used to obtain approximate formulae for the aerodynamic derivatives of simple wedge aerofoils for a wide range of Mach number and incidence. The correlation allows equilibrium real gas effects to be included in an approximate manner.

A.R.C. C.P. No. 864  
March 1965  
Squire, L. C.

APPROXIMATE FORMULAE FOR THE LIFT AND  
DRAG OF WEDGE AEROFOIL SECTIONS AT  
HIGH SUPERSONIC SPEEDS

In this paper a correlation derived by Bertram & Cook is used to obtain approximate formulae for the aerodynamic derivatives of simple wedge aerofoils for a wide range of Mach number and incidence. The correlation allows equilibrium real gas effects to be included in an approximate manner.





© Crown copyright 1966

Printed and published by

HER MAJESTY'S STATIONERY OFFICE

To be purchased from

49 High Holborn, London W.C.1

423 Oxford Street, London W.1

13A Castle Street, Edinburgh 2

109 St. Mary Street, Cardiff

Brazenose Street, Manchester 2

50 Fairfax Street, Bristol 1

35 Smallbrook, Ringway, Birmingham 5

80 Chichester Street, Belfast 1

or through any bookseller

*Printed in England*